

RESEARCH PAPER

Modified Y_2O_3 -coated biosilica with Dysprosium nanomaterials: synthesis, characterization, and optical study with enhanced catalytic activity

Younes Hanifehpour

Department of chemistry, Sayyed Jamaledin Asadabadi University, Asadabad, Iran

ARTICLE INFO

Article History:

Received 12 January 2021

Accepted 05 March 2021

Published 15 March 2021

Keywords:

Sono-photocatalytic degradation

Dysprosium

Biosilica

Luminescent

Reactive Blue 19

ABSTRACT

Dy-doped Y_2O_3 coated biosilica nanostructures with variable Dy^{3+} contents were synthesized by a facile hydrothermal technique. The products were characterized by means of energy dispersive X-ray photoelectron spectroscopy (EDX), scanning electron microscopy (SEM), X-ray diffraction (XRD), Brunauer-Emmett-Teller (BET), UV-Vis diffuse reflectance spectroscopy, and photoluminescence spectroscopy techniques. XRD demonstrated that the particles were crystallized excellently and attributed to the cubic phase of Y_2O_3 . The substitution of Dy^{3+} ions into Y_2O_3 lattice caused a redshift in the absorbance and a decrease in the band gap of as-prepared coated compounds. The pore volume and BET specific surface area of Dy-doped Y_2O_3 -coated diatomite were greater than uncoated biosilica. The sonophotocatalytic activities of as-synthesized specimens were evaluated for the degradation of Reactive Blue 19. The effect of various specifications such as ultrasonic power, various scavenger, and catalyst amount was investigated. The results revealed that diatomite coated with Dy^{3+} -incorporated yttrium oxide nanoparticles could be utilized in various experimental cycles with no significant decrease in photocatalytic activity.

How to cite this article

Hanifehpour Y. Modified Y_2O_3 -coated biosilica with Dysprosium nanomaterials: synthesis, characterization, and optical study with enhanced catalytic activity. *Nanochem Res*, 2021; 6(1):122-134. DOI: 10.22036/ncr.2021.01.012

INTRODUCTION

The Degradation of hazardous organic contaminants in industrial wastewater through AOPs (advanced oxidation processes) has attracted a great deal of research attention. Production of $\bullet OH$ radicals is the primary mechanism of AOPs, which have higher oxidization potential and can help to obtain efficient and faster degradation of the pollutants. The AOP process is particularly suitable for cleaning up non-degradable or toxic materials, such as petroleum constituents, pesticides, volatile organic compounds in wastewater, and aromatics [1-4].

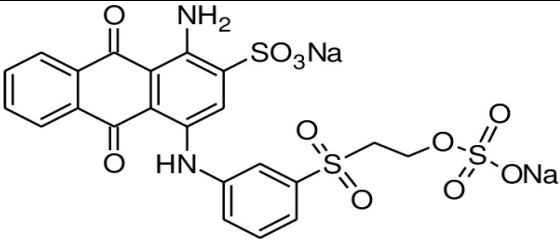
Sonocatalysis is one type of AOPs that has recently been applied for degrading organic dyes [5-7]. The chemical influence of ultrasound (US)

is caused by acoustic cavitation, leading to the formation, growth, and collapse of bubbles within a solution. By collapsing the bubbles, localized hot spots are produced with very high pressure and temperature. Due to such severe circumstances, the water molecules and dissolved oxygen undergo direct thermal dissociation to create highly reactive radical species including $\bullet OH$, oxygen ($\bullet O$), and hydrogen ($\bullet H$), which, in turn, play a pivotal role in oxidizing organic pollutants in water [8-11].

The combination of sonocatalysis and photocatalysis appears to improve the degradation share of organic pollutants owing to synergistic effects [12]. In addition to the formation of reactive oxygen species (ROS) through cavitation, the use of US in photocatalytic processes has a number of other benefits; these include incrementing the

* Corresponding Author Email: younes.hanifehpour@gmail.com

Table 1. The characteristics of C.I. Reactive blue 19

Chemical structure	
Color index name	Reactive Blue 19
Molecular formula	$C_{22}H_{16}N_2Na_2O_{11}S_3$
Color index number	219-949-9
λ_{max} (nm)	592
M_w (g/mol)	626.54

active surface area of the catalyst (by preventing the aggregation of particles, increasing the pollutants' mass transfer between the solution and catalyst surfaces), preventing catalyst deactivation (by means of continuously cleaning adsorbed molecules from the catalyst surface by micro streaming and micro bubbling), and incrementing the number of high pressure and temperature regions (through breaking up microbubbles made via the US into smaller ones in the presence of catalyst particles) [12–14].

Diatomite (diatomaceous earth), fossilized diatoms, is already used as adsorbent and carrier material. In addition, the porous structure of diatom makes it a potential heterogeneous catalyst [15–17]. Yttrium oxide (Y_2O_3) is an essential engineering compound in various fields due to its physical and chemical properties, including relatively large band gap energy, high melting point, and high permittivity [18, 19]. It has been extensively utilized in luminescent devices and transparent ceramics. To obtain better material performance, many investigations have been conducted on controlling the morphology and size of Y_2O_3 . Yttria has found many high-technology applications because of its well-defined crystal structures and outstandingly high affinity for oxygen and sulfur; these properties can be qualified by substituting different kinds of ions into the lattice [20]. Lanthanide-doped nanostructured semiconductors have recently been used as active photocatalysts and sonocatalyst. Rare earth cations with empty 5d orbitals and partly occupied 4f orbitals could also notably enhance the separation rate of photo-induced charge carriers within semiconductor sonocatalysts and improve significantly the sonocatalytic activity [1,21–23].

However, no report exists on the sonocatalytic degradation of Reactive Blue 19 (RB 19) in the presence of coated-diatom with dysprosium-doped Y_2O_3 .

This study aimed to describe a simple hydrothermal route for the preparation of coated-diatom with dysprosium-doped Y_2O_3 ($Dy_xY_{2-x}O_3$) nanomaterials. We assessed the nanoparticles' sonocatalytic activity for RB 19 (see Table 1). In addition, we examined and optimized the sonophotocatalytic degradation of organic dye. We also investigated the influence of inorganic ions on the degradation effectiveness of RB19.

EXPERIMENTAL METHODS

Chemicals and materials

The chemicals used in this study had analytical grades and were utilized with no further purification. Diatomaceous earth (97.5% SiO_2), YCl_3 (99.99%), ethanol (99%), and $Dy(NO_3)_3 \cdot 5H_2O$ were purchased from Sigma-Aldrich. RB19 was acquired from the Zhejiang Yide Chemical Company (China).

Characterization

The samples' crystal phase composition was determined using XRD characterization at room temperature through a D8 Advance diffractometer (Bruker, Karlsruhe, Germany) with monochromatic high-intensity Cu $K\alpha$ radiation ($\lambda=1.5406 \text{ \AA}$), an emission current of 30 mA, and accelerating voltage of 40 kV. Elemental analyses were obtained using a linked ISIS-300, (Oxford Instruments, Abingdon, UK) (energy dispersion spectroscopy) detector. Using an electron microscope (SEM, S-4200, Hitachi, Tokyo, Japan), the surface state and the

morphology were observed. A diffuse reflectance UV-Vis spectrophotometer was utilized to obtain the samples' optical absorption spectra (Varian Cary 3 Bio, Varian Ltd., Artarmon, Australia). The specific surface areas were measured through a single point BET technique utilizing Micrometrics Gemini V and Gemini 2375. Cell parameters were calculated with the Celref program from powder XRD patterns, and reflections were determined and fitted using a profile fitting procedure with the Winxpow program. The reflections observed in $2\theta = 10\text{--}70^\circ$ were used for the lattice parameter determination.

Preparation of Dy-doped Y_2O_3 nanoparticles

Dy-doped yttrium oxide compounds with different Dy contents (0–8 mol%) were made hydrothermally. In a typical synthesis, first, Dy (NO_3) $_3 \cdot 5H_2O$ and proper molar ratios of YCl_3 were dissolved in 30 ml of deionized water. Next, EDTA (0.3 g) and 1 mmol NaOH were added dropwise to the solution while stirring it at moderate speed. The above solution was transferred into 100-ml autoclave with Teflon-lined stainless-steel. Then it was settled in an oven at $230^\circ C$ for 48 h and finally allowed to cool naturally to room temperature. Gathering the as-prepared $Dy_xY_{2-x}O_3$ nanoparticles, they were rinsed numerous times with absolute ethanol and distilled water to remove residual impurities, and then dried at vacuum for 2 h at $55^\circ C$. The result was a white powder.

Diatomite coated with Dy-doped Y_2O_3 nanoparticles

The diatom was weighted and added to 25mL deionized water and was continuously stirred to spread evenly. Then, 1 g Dy-doped Y_2O_3 compounds with various Dy content were added to the above solution to fully disperse. After 1 hour ultrasonic irradiation, the solution was transferred into a 100-ml autoclave with Teflon-lined stainless-steel, settled in an oven at $140^\circ C$ for 10 h and then cooled down naturally to room temperature. The final coated-diatom was obtained after washing and drying the precipitates at $60^\circ C$.

Evaluation of catalytic activity

The sonophotocatalytic activity of the diatom biosilica coated with Dy-doped yttria nanomaterial was assessed to decolorize of RB19 as a model organic pollutant. Within a characteristic procedure, suspending the nanocatalyst (0.1 g) was performed in an aqueous solution of the model dye

(100 mL) with an identified initial concentration at $pH=6.5$. Then, the suspension was irradiated by a 40W compact fluorescent visible lamp armed with a cutoff filter to present visible light illumination (λ of higher than 420 nm) into the ultrasonic bath. A UV-Vis spectrophotometer was utilized to determine the removal of dye via the absorbance at $\lambda_{max} = 592$ nm. The decolorization efficiency (DE) was determined as follows:

$$DE(\%) = \left(1 - \frac{C}{C_0}\right) \times 100 \quad (1)$$

where C and C_0 are the dye's final and initial concentrations within the solution (mg/L), respectively. To test the nanocatalyst's reusability, the utilized catalyst was separated from the solution, rinsed with distilled water, and utilized in a fresh test after drying at $70^\circ C$.

RESULTS AND DISCUSSION

Characterizing the synthesized samples

Fig. 1 presents the XRD pattern of uncoated diatomite, Y_2O_3 , and diatom-coated with Dy-doped Y_2O_3 . The diatomite XRD pattern was indexed readily to SiO_2 (JCPDS card no. 00-001-0647), while the four broad and strong peaks with attributed reflections of (222), (400), (440), (622) and $2\theta = 29.1, 33.7, 48.6$ and 58.2° were related to cubic structure of yttria, respectively (JCPDS card no. 41-1105) [24]. The indistinguishable forms of the XRD patterns of Y_2O_3 and the compounds coated with $Dy_xY_{2-x}O_3$ suggest that the surface of diatom was equally covered. As illustrated in Fig. 1, in substitution of yttria by Dy^{3+} , only the peaks related to Y_2O_3 were still noticed and no other peaks corresponding to $Y(OH)_3$, Dy_2O_3 or other impurities were detected, which demonstrates that the Dy^{3+} ions substitute Y^{3+} ions in the yttria structure. A slight shift was found to lower diffraction for diatomite-coated with Dy-doped Y_2O_3 samples.

The cell parameters of the synthesized materials were calculated from the XRD patterns. By increasing dopant content (x), a, b and c parameters for Dy^{3+} increased (Fig. 2). The trend for lattice constants could be correlated to the effective ionic radii of the Ln^{3+} ions, which resulted in greater amount of lattice parameters for Dy^{3+} doped materials.

Fig. 3 displays SEM images of the diatom-

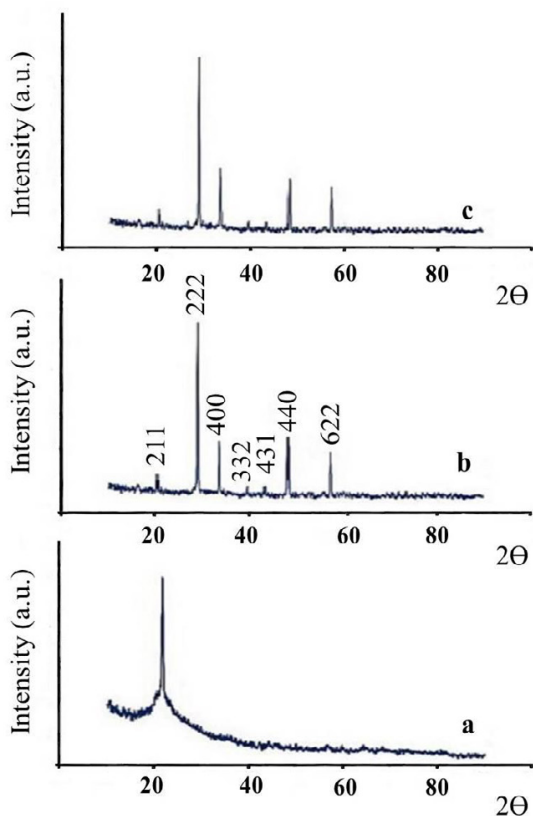


Fig. 1. The XRD pattern of diatomite (a), Y_2O_3 (b), diatom-coated with 6% Dy-doped Y_2O_3 (c) and diatom-coated with 8% Dy-doped Y_2O_3 (d) nanoparticles

coated with 6% Dy-doped Y_2O_3 and uncoated sample produced by the hydrothermal route. The skeletal-remain biosilica with high porosity structure is shown in Fig. 3a. High porosity and the surface morphology of diatom can be employed as a template to enhance the potential of functional materials. Fig. 3b represents the image of 6% Dy-doped Y_2O_3 nanoparticles, the diameter of which was around 25–70nm. Following the immobilization of 6% Dy-doped yttrium oxide, the SEM image of diatomite is seen in Fig 3c, d. Changing the mass ratio of the substrate–diatomite and the coating material–doped- Y_2O_3 controlled the thickness of the coating layers. To achieve smooth, stable and uniform coating, the optimum ratio was 1.5.

The elemental mapping of O, Y, Dy and Si in the diatom-coated with Dy-doped Y_2O_3 sample is shown in Table 2 confirming the XRD outcome.

Fig. 4a shows the absorbance spectra of Dy-doped Y_2O_3 coated diatomite compounds. A

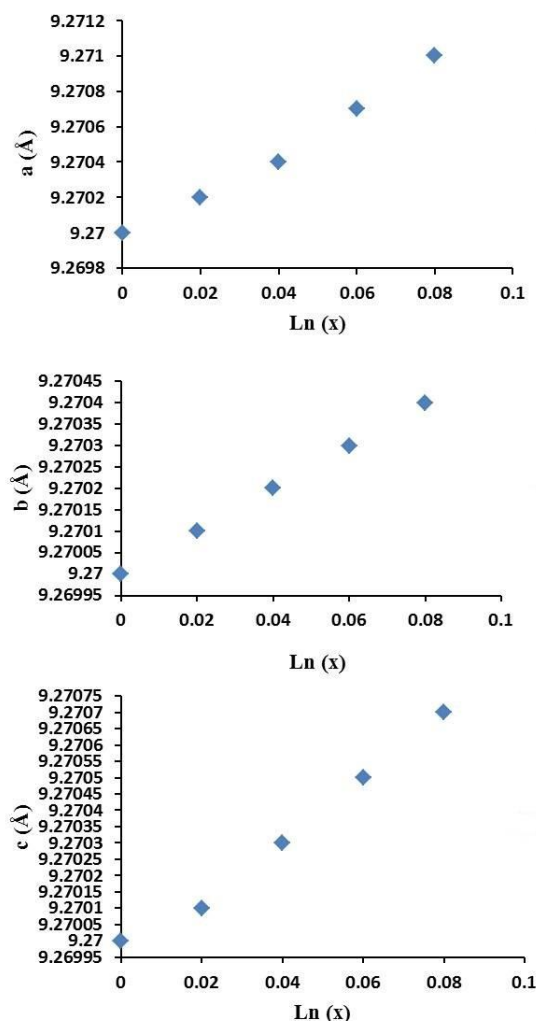


Fig. 2. The lattice constant of $Dy_xY_{2-x}O_3$ ($x = 0$ to 0.08) dependent upon Dy^{3+} doping on Y^{3+} sites

redshift in absorbance spectra is seen by increasing dopant content.

The as-prepared compound's band gap energy can be determined from the interception of the resultant linear area with the energy axis according to $(h\nu\alpha)^2$ versus $(h\nu)$ (Tauc plot)(Fig.4b). The doped Y_2O_3 had lower E_g values compared to the pure sample, which were reduced by increasing the dopant. Table 3 lists the band gap energy for Dy-doped Y_2O_3 coated diatomite nanoparticles.

Adsorption/desorption isotherm of nitrogen for uncoated and coated diatomite with 6% dy^{3+} -substituted Y_2O_3 are shown in Fig. 5. In the case of both specimens, two isotherms with obvious hysteresis loop were noticed in the pressure range of 0.3–1.0 p/p_0 . The BET specific surface area of biosilica is 1.65 m^2/g . Additionally, the BET specific

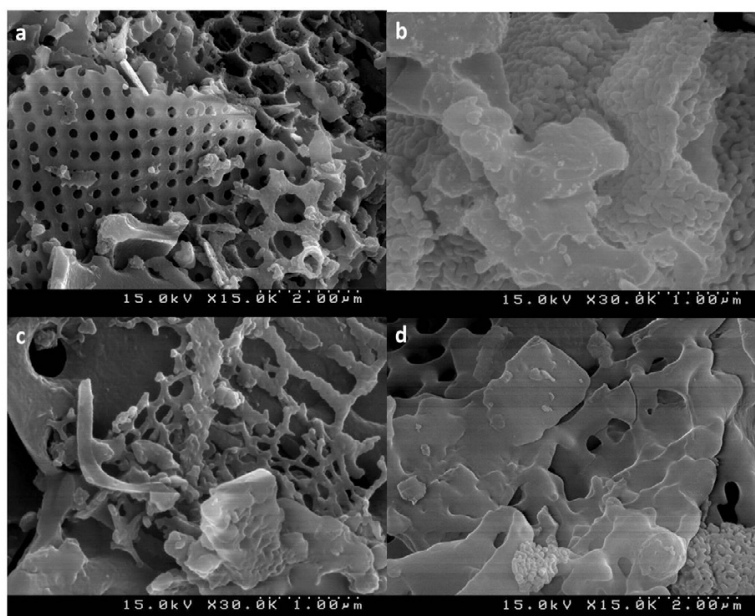


Fig. 3. SEM images of natural diatomite (a), 6% Dy-doped Y_2O_3 (b) and 6% Dy-doped Y_2O_3 -coated diatomite at different magnification (c,d)

Table 2. The atomic percent of 6% Dy-doped Y_2O_3 -coated diatomite.

Element	Line Type	Wt%	Atomic %	Factory Standard
O	K series	56.50	67.38	Yes
Si	K series	37.50	29.37	Yes
Y	L series	4.86	2.31	Yes
Dy	M series	1.14	0.94	Yes
Total:		100.00	100.00	

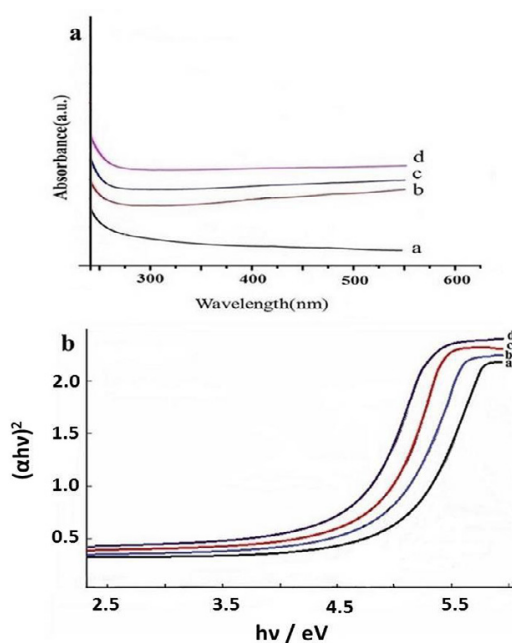
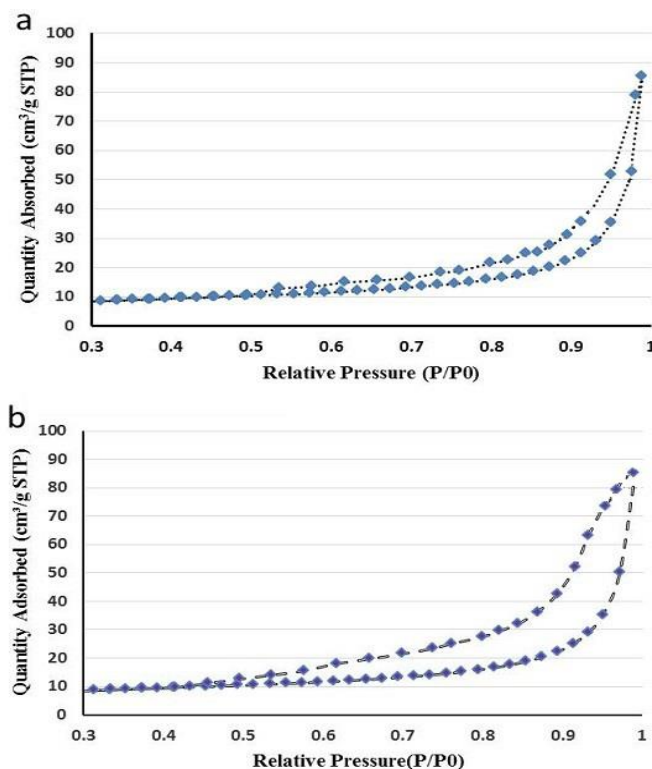


Fig.4. Absorbance spectra of diatom coated with Y_2O_3 (a), diatom coated with 4% Dy-doped Y_2O_3 (b), diatom coated with 6% Dy-doped Y_2O_3 (c) and diatom coated with 8% Dy-doped Y_2O_3 (d) at room temperature

Table 3. Band gap energy of diatom coated with Eu-doped Y_2O_3 nanostructures.

Sample	Band gap (eV)
Diatom coated with Y_2O_3	4.93
diatom coated with 4%Dy-doped Y_2O_3	4.74
diatom coated with 6%Dy-doped Y_2O_3	4.66
diatom coated with 8%Dy-doped Y_2O_3	4.55

Fig.5. Adsorption–desorption isotherm of nitrogen for diatomite (a) and diatom coated with 6% Dy-doped Y_2O_3 (b)

surface area of diatomite coated with 6% Dy-substituted Y_2O_3 ($8.85 \text{ m}^2/\text{g}$) considerably exceeds that of uncoated diatom. A superior adsorption performance is expected for coated-diatom with dysprosium-doped Y_2O_3 nanoparticles.

Synergistic effect of photocatalysis and sonocatalysis on the degradation of RB19 using diatomite coated with Dy-doped Y_2O_3 nanoparticles

Through some comparative tests, the sonocatalytic, photocatalytic, and sono-photocatalytic behaviors of the synthesized diatomite coated with Dy-doped Y_2O_3 were determined, for which the findings are presented in Fig. 6. The decolorization efficiency was negligible in the absence of the catalyst particles under light

irradiation, which shows that photolysis does not contribute to the RB19 removal from the aqueous solution.

The results of the test conducted in dark conditions revealed that surface adsorption have no significant effect on decolorizing the dye solution. The removal percentage by the photocatalytic procedure was less than 66%. The decolorization efficiency by sonocatalytic degradation (50%) was greater than that of the sonolysis process (7%). The decolorization efficiency was significantly improved in the sono-photocatalytic process (94.15%) as a result of synergistic impacts between sonocatalysis and photocatalysis. This can be summarized as: first, the generation of several ROSs through the integrated photocatalytic procedure and cavitation

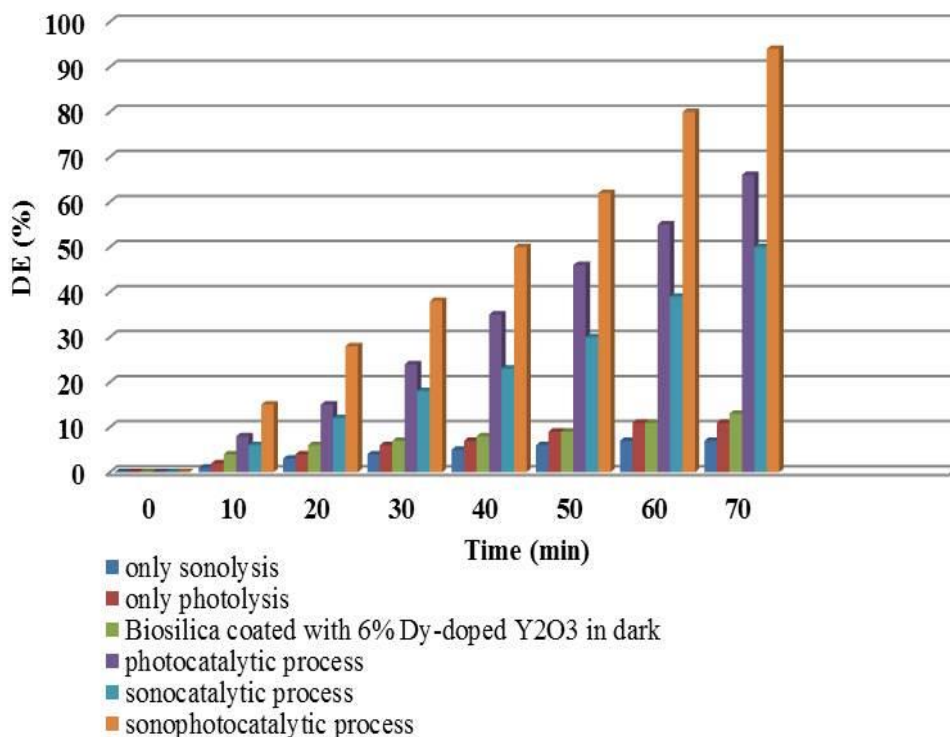


Fig. 6. Comparison of different catalytic processes in decolorization of Reactive blue 19

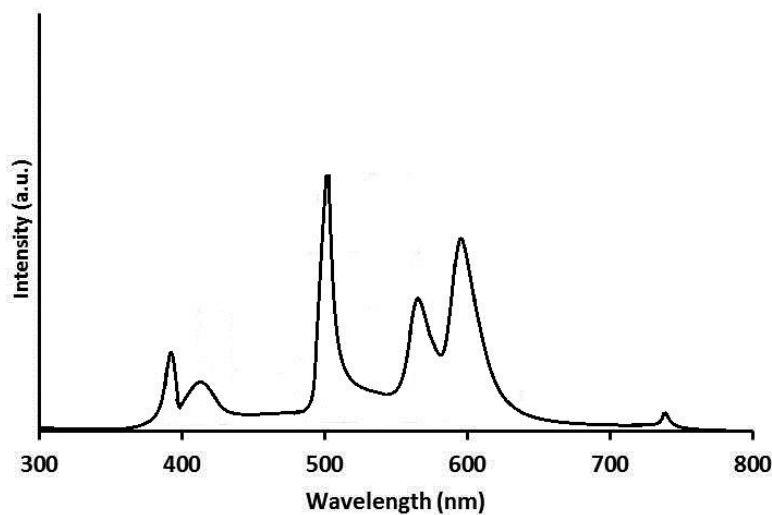


Fig.7. The spectra of the lamp used for catalytic process

effects; second, the improved mass transfer rates; third, the catalyst particles disaggregation through US and the larger active surface areas; and fourth, the creation of more hot spots by existing catalyst particles [12–14]. Fig. 7 indicates the spectra of the

lamp used for catalytic process.

As demonstrated in Fig. 8, the graph of $(-ln(C/C_0))$ vs. time indicates linear dependence for all three sono-photocatalytic, photocatalytic and sonocatalytic processes, displaying pseudo-

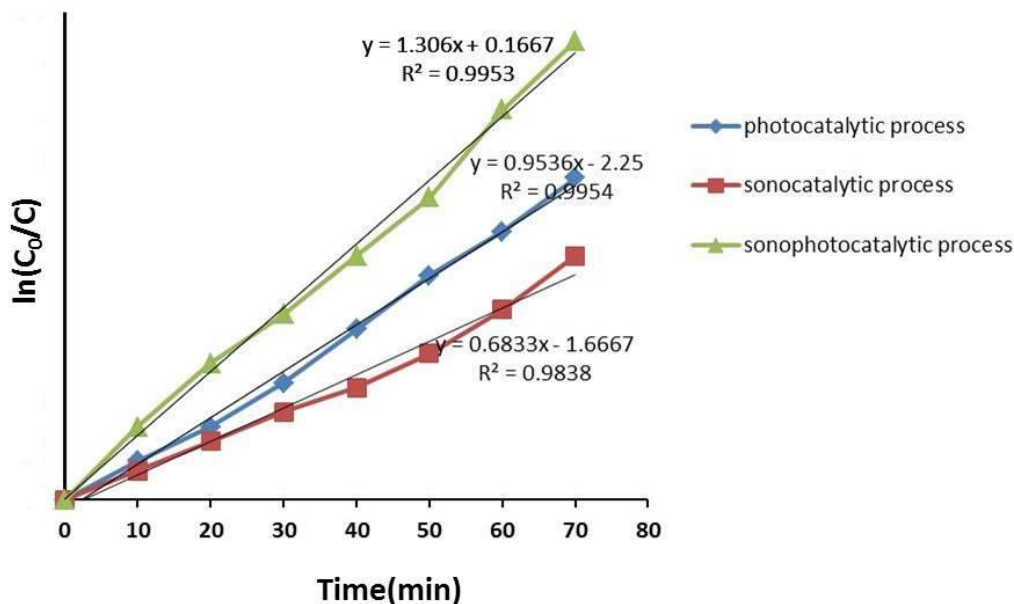


Fig.8. First-order kinetic plot for sono-photocatalytic, sonocatalytic and photocatalytic processes. [Dye] = 20 mg/L, [Catalyst] = 1.25 g/L

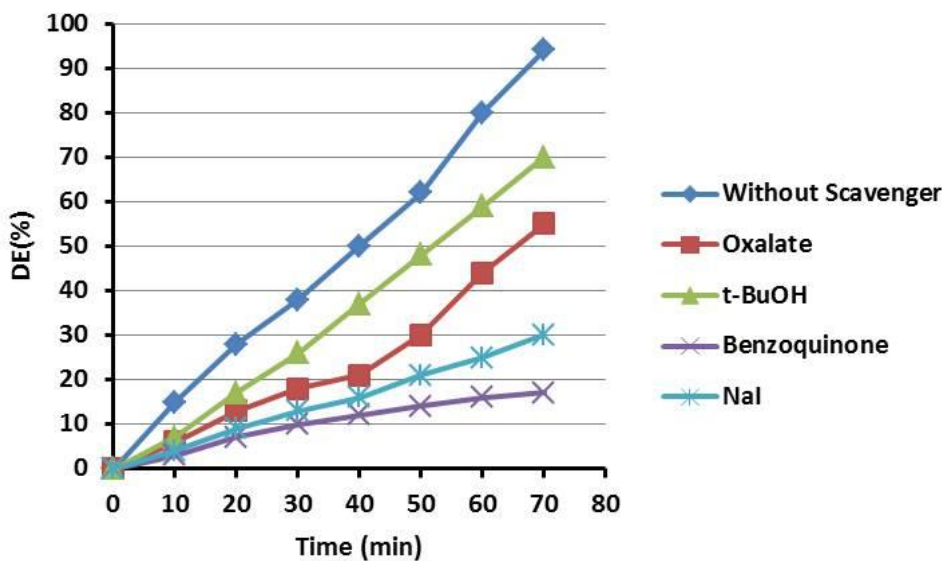


Fig. 9. The effects of various scavengers on decolorizing of Reactive Blue 19, [Dye] = 20 mg/L, [Catalyst] = 1.25 g/L, pH= 6.5, [Scavenger] = 5 mM

first-order kinetics [1, 25]. It is obvious that the decolorization efficiency and pseudo-first-order kinetic constant in sono-photocatalysis ($k_{obs, sono-photo}$) are greater than those for photocatalysis ($k_{obs, photo}$) and sonocatalysis ($k_{obs, sono}$). These results implicitly include the concept of a synergistic effect.

To assess the degradation process's mechanism

and to discover the main oxidative species, experiments were conducted in the presence of appropriate scavengers of active species. According to Fig. 9, adding t-BuOH (a scavenger of hydroxyl radicals) led to a reduction of 14% in the decolorization percentage. By adding oxalate (a scavenger of h^+_{VB}), the decolorization percentage

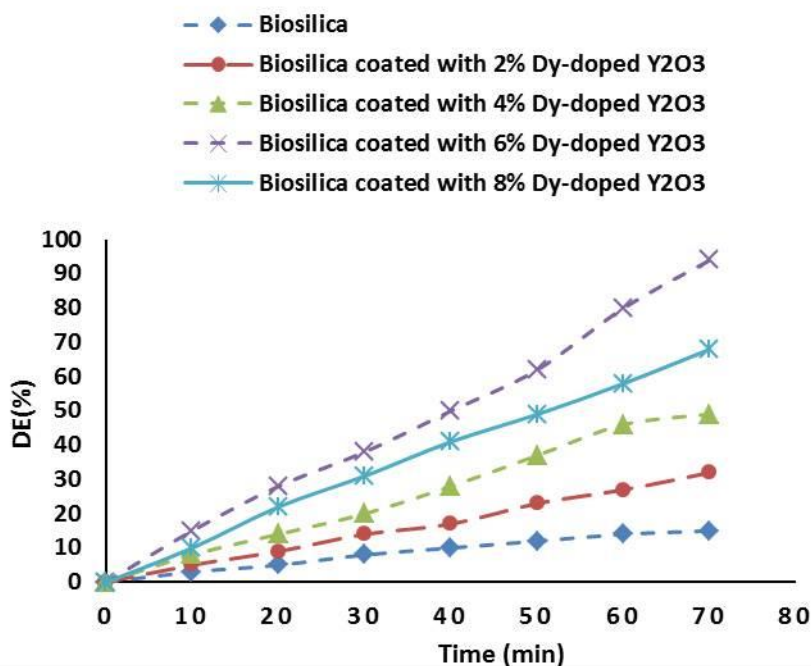
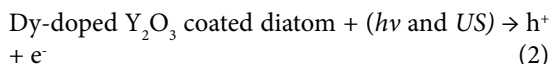


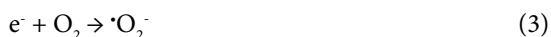
Fig.10. The decolorization of RB19 with different Dy³⁺ content (catalyst loading 1.25 g/L)

decreased to 54%. In the case of I⁻ (scavenger of hole), it reached 30%. When benzoquinone (BQ) was added (a scavenger of superoxide radicals), the dye degradation was inhibited remarkably. Such findings indicate that the h^+_{VB} and superoxide radicals are the main oxidative species in degrading dye molecules although the hydroxyl radicals also affect the decolorization. Regarding the synergistic impacts of sonocatalysis and photocatalysis, a possible mechanism for the degradation procedure can be suggested [12,14]:

1) Both US and light irradiation can excite the catalyst nanoparticles to form electron-hole pairs:



2) The conduction-band electrons can react with adsorbed oxygen molecules to create $\cdot O_2^-$, $HO_2\cdot$, and H_2O_2 :



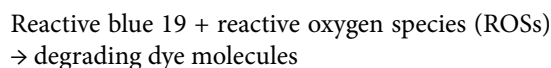
3) Hydroxyl anions or water molecules can be oxidized by the photogenerated holes to form hydroxyl radicals:



4) The water molecule pyrolysis can be promoted by the existence of ultrasonic irradiation to produce hydrogen and hydroxyl radicals:



5) Ultimately, the dye molecules can be degraded by the created active species:



Effect of Dy³⁺ Content of diatom coated Dy-doped Y₂O₃ Nanoparticles

The removal effectiveness of RB 19 over diatomite coated Dy-doped Y_2O_3 sonocatalysts during 70 min of sonophotolysis is shown in Fig. 10. The doped samples with proper content of

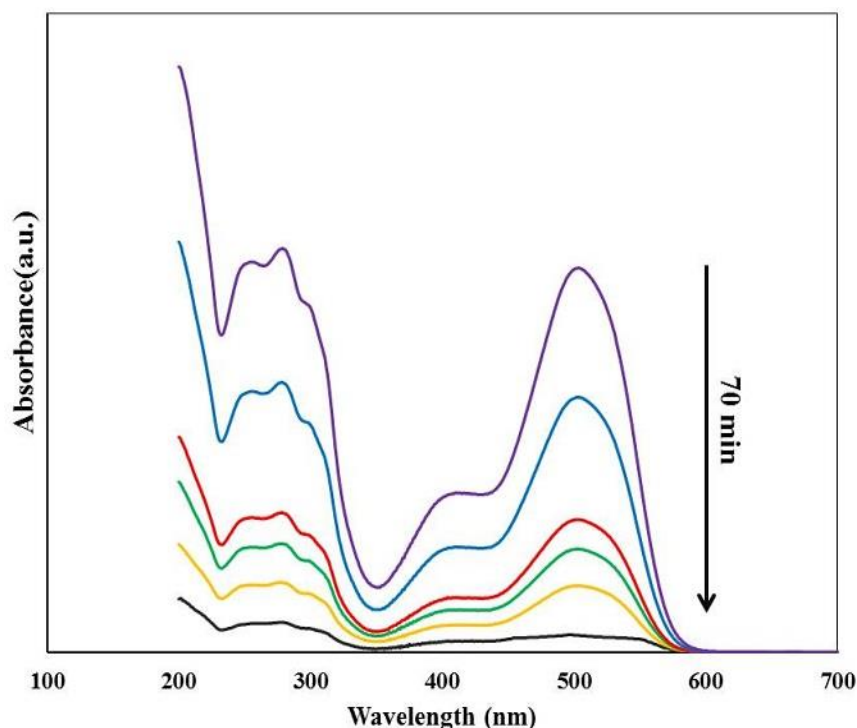
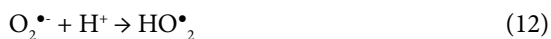


Fig.11. Degradation of Reactive blue 19 under ultrasonic irradiation using diatomite coated with 6% Dy-doped yttrium oxide

Dy³⁺ ion had much better catalytic performance compared with uncoated biosilica. For diatom coated 6 % Dy doped Y₂O₃ nanoparticles, the highest decolorization efficiency was achieved. Two mechanisms can explain these findings. First, rare-earth cations like Dy³⁺ restrain the electron-hole recombination and act as an electron scavenger. Second, the new energy level under the conduction band edge of Y₂O₃ is created by the substitution of Dy³⁺ into yttria lattice [26].



•OH, H₂O₂ and O₂[•] radicals are well-known powerful oxidants for the degradation of organic dye [27].

The UV-Vis absorption spectra of RB 19 at various irradiation periods for the sonophotocatalytic process are shown in Fig.

11. Reducing the concentration of RB 19 during the catalytic process is used to examine the performance of the catalyst.

Effect of sonication energy

The decolorization percentage of RB19 under different ultrasonic power in the range of 60 to 150 W was also investigated. Employing the sonication power of 50 to 150 W/L, the degradation percentage increased from 81.32 % to 94 % (Fig.12). Enhanced degradation ratio was achieved through increasing the ultrasonic power, which increased the production of •OH radicals. Moreover, the disturbance of the solution was elevated with significant power, which accordingly promoted the mass transfer rate of dye, reactive species and intermediates between catalyst's surface and the bulk solution [28]. In order to save energy, the experiments were set on 120 W due to slight contrast of degradation percentage between 120 and 150 W.

Photocatalyst recycling and photostability

Fig. 13 displays the reusability of diatomite coated 6% Dy-doped yttrium oxide, which

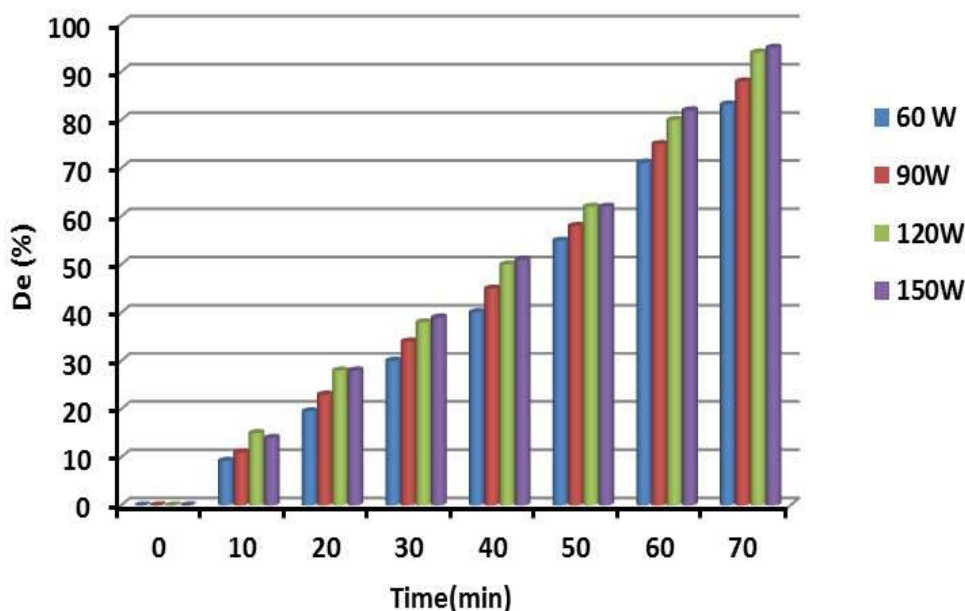


Fig. 12. Ultrasound power effect on the degrading RB 19 by diatomite coated 6 % Dy-doped Y_2O_3 , [Catalyst]₀ = 1.25 g/L, pH=6.5 and [RB 19]₀ = 20 mg/L

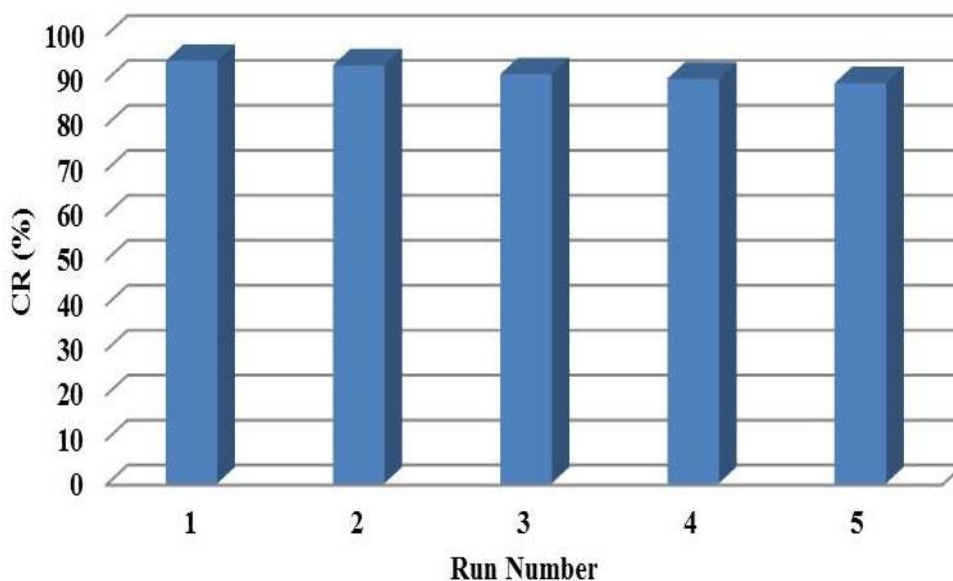


Fig.13. Reusability of the diatomite coated 6% Dy-doped yttrium oxide nanostructures within five continuous experiments. The ultrasonic power = 120 W/L, [Catalyst]₀ = 1.25 g/L, [RB 19]₀ = 20 mg/L, pH=6.5 and the reaction time = 70 min

was tested at a reaction period of 70 min, a dye concentration of 20 mg/L, and 1.25 g/L of catalyst powder. These conditions were the optimum operational parameters confirmed by the experiments. After five repeated runs, the decrease in the sono-photocatalytic process was negligible,

which confirms the synthesized nanoparticles' reusability and high potential stability.

CONCLUSION

Dysprosium-doped Y_2O_3 -coated diatomite nanomaterials were prepared using a facile

hydrothermal route and employed for the degradation of reactive blue 19 in an aqueous solution. The substitution of Dy^{3+} into yttrium oxide lattice led to a redshift in absorbance spectra and reduction of band gap, respectively. The decolorization effectiveness of the synthesized compounds was much higher in sono-photocatalytic process than that of other methods. 6% Dy^{3+} -incorporated Y_2O_3 coated diatom exhibited the best degradation ratio. Radical scavengers reduced the sonophotocatalytic degradation percentage of R B 19 particularly subject to 1,4 benzoquinone. The results revealed that diatomite coated with Dy^{3+} -incorporated yttrium oxide nanoparticles can be utilized in various experimental cycles with no significant drop in photocatalytic activity.

ACKNOWLEDGMENTS

This work was funded by the Sayyed Jamaledin Asadabadi University.

CONFLICTS OF INTEREST

The authors declare no conflict of interest.

REFERENCES

- Hanifehpour Y, Soltani B, Amani-Ghadim AR, Hedayati B, Khomami B, Joo SW. Synthesis and characterization of samarium-doped ZnS nanoparticles: A novel visible light responsive photocatalyst. *Materials Research Bulletin*. 2016;76:411-21.
- Ahmed S, Rasul MG, Martens WN, Brown R, Hashib MA. Heterogeneous photocatalytic degradation of phenols in wastewater: A review on current status and developments. *Desalination*. 2010;261(1-2):3-18.
- Yuan B, Wang Y, Bian H, Shen T, Wu Y, Chen Z. Nitrogen doped TiO₂ nanotube arrays with high photoelectrochemical activity for photocatalytic applications. *Applied Surface Science*. 2013;280:523-9.
- Daghrir R, Drogui P, Deegan N, El Khakani MA. Electrochemical degradation of chlortetracycline using N-doped Ti/TiO₂ photoanode under sunlight irradiations. *Water Research*. 2013;47(17):6801-10.
- Khataee A, Karimi A, Arefi-Oskoui S, Darvishi Cheshmeh Soltani R, Hanifehpour Y, Soltani B, et al. Sonochemical synthesis of Pr-doped ZnO nanoparticles for sonocatalytic degradation of Acid Red 17. *Ultrasonics Sonochemistry*. 2015;22:371-81.
- Eskandarloo H, Badiie A, Behnajady MA, Ziarani GM. Ultrasonic-assisted sol-gel synthesis of samarium, cerium co-doped TiO₂ nanoparticles with enhanced sonocatalytic efficiency. *Ultrasonics Sonochemistry*. 2015;26:281-92.
- Khataee AR, Karimi A, Soltani RDC, Safarpour M, Hanifehpour Y, Joo SW. Europium-doped ZnO as a visible light responsive nanocatalyst: Sonochemical synthesis, characterization and response surface modeling of photocatalytic process. *Applied Catalysis A: General*. 2014;488:160-70.
- Saharan P, Chaudhary GR, Lata S, Mehta SK, Mor S. Ultra fast and effective treatment of dyes from water with the synergistic effect of Ni doped ZnO nanoparticles and ultrasonication. *Ultrasonics Sonochemistry*. 2015;22:317-25.
- Villaroel E, Silva-Agredo J, Petrier C, Tabora G, Torres-Palma RA. Ultrasonic degradation of acetaminophen in water: Effect of sonochemical parameters and water matrix. *Ultrasonics Sonochemistry*. 2014;21(5):1763-9.
- Bansal P, Chaudhary GR, Mehta SK. Comparative study of catalytic activity of ZrO₂ nanoparticles for sonocatalytic and photocatalytic degradation of cationic and anionic dyes. *Chemical Engineering Journal*. 2015;280:475-85.
- Chakma S, Moholkar VS. Investigation in mechanistic issues of sonocatalysis and sonophotocatalysis using pure and doped photocatalysts. *Ultrasonics Sonochemistry*. 2015;22:287-99.
- Anju SG, Yesodharan S, Yesodharan EP. Zinc oxide mediated sonophotocatalytic degradation of phenol in water. *Chemical Engineering Journal*. 2012;189-190:84-93.
- Khataee A, Saadi S, Safarpour M, Joo SW. Sonocatalytic performance of Er-doped ZnO for degradation of a textile dye. *Ultrasonics Sonochemistry*. 2015;27:379-88.
- Khataee A, Soltani RDC, Karimi A, Joo SW. Sonocatalytic degradation of a textile dye over Gd-doped ZnO nanoparticles synthesized through sonochemical process. *Ultrasonics Sonochemistry*. 2015;23:219-30.
- Agdi K, Bouaid A, Esteban AM, Hernando PF, Azmani A, Camara C. Removal of atrazine and four organophosphorus pesticides from environmental waters by diatomaceous earth-remediation method. *Journal of Environmental Monitoring*. 2000;2(5):420-3.
- Alvarez E, Blanco J, Avila P, Knapp C. Activation of monolithic catalysts based on diatomaceous earth for sulfur dioxide oxidation. *Catalysis Today*. 1999;53(4):557-63.
- Li F, Xing Y, Huang M, Li KL, Yu TT, Zhang YX, et al. MnO₂ nanostructures with three-dimensional (3D) morphology replicated from diatoms for high-performance supercapacitors. *Journal of Materials Chemistry A*. 2015;3(15):7855-61.
- Wilk GD, Wallace RM, Anthony JM. High-κ gate dielectrics: Current status and materials properties considerations. *Journal of Applied Physics*. 2001;89(10):5243-75.
- Basavegowda N, Mishra K, Thombal RS, Kaliraj K, Lee YR. Sonochemical Green Synthesis of Yttrium Oxide (Y₂O₃) Nanoparticles as a Novel Heterogeneous Catalyst for the Construction of Biologically Interesting 1,3-Thiazolidin-4-ones. *Catalysis Letters*. 2017;147(10):2630-9.
- McN. Alford N, Birchall JD, Clegg WJ, Harmer MA, Kendall K, Jones DH. Physical and mechanical properties of YBa₂Cu₃O_{7-δ} superconductors. *Journal of Materials Science*. 1988;23(3):761-8.
- Hanifehpour Y, Soltani B, Amani-Ghadim AR, Hedayati B, Khomami B, Joo SW. Praseodymium-doped ZnS nanomaterials: Hydrothermal synthesis and characterization with enhanced visible light photocatalytic activity. *Journal of Industrial and Engineering Chemistry*. 2016;34:41-50.
- Khataee A, Khataee A, Fathinia M, Hanifehpour Y, Joo SW. Kinetics and Mechanism of Enhanced Photocatalytic Activity under Visible Light Using Synthesized PrxCd_{1-x}Se Nanoparticles. *Industrial & Engineering Chemistry Research*. 2013;52(37):13357-69.
- Hamnabard N, Hanifehpour Y, Khomami B, Woo Joo S. Synthesis, characterization and photocatalytic performance of Yb-doped CdTe nanoparticles. *Materials Letters*. 2015;145:253-7.
- Qipeng L, Yanbing H, Aiwei T, Zhihui F, Feng T, Xiaojun

- L. Synthesis and Characterization of $Y_2O_3:Er^{3+}$ Upconversion Materials with Nanoporous Structures. *Journal of Nanoscience and Nanotechnology*. 2011;11(11):9671-5.
25. Daneshvar H, Seyed Dorraji MS, Amani-Ghadim AR, Rasoulifard MH. Enhanced sonocatalytic performance of ZnTi nano-layered double hydroxide by substitution of Cu (II) cations. *Ultrasonics Sonochemistry*. 2019;58:104632.
26. Alemi A, Hanifehpour Y, Joo SW, Min B-K. Synthesis of novel $Ln_xSb_{2-x}Se_3$ (Ln: Lu^{3+} , Ho^{3+} , Nd^{3+}) nanomaterials via co-reduction method and investigation of their physical properties. *Colloids and Surfaces A: Physicochemical and Engineering Aspects*. 2011;390(1-3):142-8.
27. Korake PV, Kadam AN, Garadkar KM. Photocatalytic activity of Eu^{3+} -doped ZnO nanorods synthesized via microwave assisted technique. *Journal of Rare Earths*. 2014;32(4):306-13.
28. Hou L, Zhang H, Wang L, Chen L. Ultrasound-enhanced magnetite catalytic ozonation of tetracycline in water. *Chemical Engineering Journal*. 2013;229:577-84.